

# Validation of fluid-structure interaction simulation environment in analysis of large-break loss of coolant accident

Tellervo Brandt, Ville Lestinen, Timo Toppila, Jukka Kähkönen, Antti Timperi, Timo Pättikangas, Ismo Karppinen

**Abstract—** In this article, we study a large-break loss of coolant accident (LBLOCA) where a guillotine break of one of the main coolant pipes occurs near the reactor pressure vessel (RPV). This initiates a pressure wave which propagates inside the RPV. The simulation of bidirectional fluid-structure interaction phenomena has been found to be important for accurate prediction of the resulting deformation and loads. In this article, fully coupled simulation results are validated against the German HDR (Heißdampfreaktor) experiments. The computational fluid dynamic (CFD) software Fluent and Star-CD are applied to modeling of three-dimensional, viscous, turbulent fluid flow. The MpCCI code is used for bidirectional coupling of the CFD simulation to the structural solver Abaqus. Pressure boundary condition at the pipe break is obtained in a two-phase simulation with the system code APROS. Comparisons are made for break mass flow, wall pressure, displacement and strain. The simulation results follow the experimental data fairly well. The sensitivity of the results to pressure boundary condition and water temperature is studied. In addition, the necessity of using bidirectional coupling instead of one-way pressure mapping is demonstrated.

## I. INTRODUCTION

LARGE-break loss of coolant accident (LBLOCA) is one of the design basis accidents of nuclear power plants (NPP). In a hypothetical accident scenario, a "guillotine" break of one of the main coolant pipes of the primary circuit causes a rapid pressure drop at the break location. The pressure transient propagates inside the reactor pressure vessel (RPV), and within the first hundreds of milliseconds after the break, the pressure loads induce deformations on the structures and threaten their integrity. In this article, the pressure transient is simulated by coupling commercial computational fluid dynamic (CFD) and structural solvers using the MpCCI interface [1]. The pressure boundary condition required in the CFD model, is calculated using the system code APROS [2]. The results are validated against the HDR (Heißdampfreaktor) experiments [3]-[5], where LBLOCA was studied in a full-scale geometry using realistic initial conditions. The main focus

here is to validate a simulation environment which can be utilized in safety analysis of the Loviisa NPP which includes two VVER-440 type pressurized water reactors (PWR) owned by Fortum Power and Heat Ltd.

In earlier studies of pressure transient resulting from the pipe break during LBLOCA, accounting for bidirectional fluid-structure interaction (FSI) phenomena has been found important (see e.g. [4], [6], [7]). FSI simulation results obtained with bidirectional coupling of CFD and structural solvers have recently been validated against the HDR experiments in [6], [8], and [9]. The HDR experiments and simulations with system codes like APROS show that the FSI problem can be simulated as a one-phase flow approximately for the first 100 ms after the break [4], [9]. However, two-phase phenomena have to be accounted for in evaluating the boundary condition at the break. A finite-element based solver was applied in [6] and [8] to account for inviscid fluid flow and structural motion. In [9], the use of an acoustic model of water included in the structural solver was compared to utilizing the Reynolds-averaged Navier-Stokes (RANS) solver Star-CD [10] for modeling of turbulent viscous fluid flow. It was found that in the case of the HDR experiments, the latter approach was required.

In the present work, the CFD solver Fluent [11] is applied together with the structural solver Abaqus [12], and the pressure at the break nozzle is taken from simulations with the system code APROS. The turbulent viscous fluid flow is simulated using the RANS approach as in the work of [9].

## II. HDR BLOWDOWN EXPERIMENTS

The HDR blowdown experiments were carried out in the early 1980's in Germany. FSI phenomena caused by the flexibility of the core barrel during the initial depressurization phase of LBLOCA were studied in particular, and one of the main emphases was to provide reference data for validation of three-dimensional FSI codes.

The lay-out and the main dimensions of the test facility are shown in Fig 1. The break occurs in the nozzle A1 shown in Fig 1. Most of the other nozzles of the reactor were closed in order to provide clear boundary conditions for CFD calculations, and the effect of those left open was estimated to be small [3]. The main parameters of the test facility are compared to those of Loviisa NPP in Table 1, and we see that the construction is quite realistic. However, a short break opening time, about 1 to 2 ms, was used in the experiments, whereas opening times of 10 - 15 ms or even longer have been proposed for a realistic break [6], [13].

Manuscript received August 8, 2008. This work was partly funded by the National Technology Agency of Finland (Tekes) within the MULTIPHYSICS project. This work is also a part of the SAFIR2010 programme (The Finnish Research Programme on Nuclear Plant Safety 2007-2010).

T. Brandt, V. Lestinen, J. Kähkönen and T. Toppila are with Fortum Nuclear Services Ltd. POB FI-00048 FORTUM, Finland (corresponding author: phone: +358 40 5425160; fax: +358 10 4533403; e-mail: tellervo.brandt@fortum.com).

A. Timperi, T. Pättikangas, and I. Karppinen are with VTT Technical Research Centre of Finland, P.O.B. 1000, FI-02044 VTT, Finland.

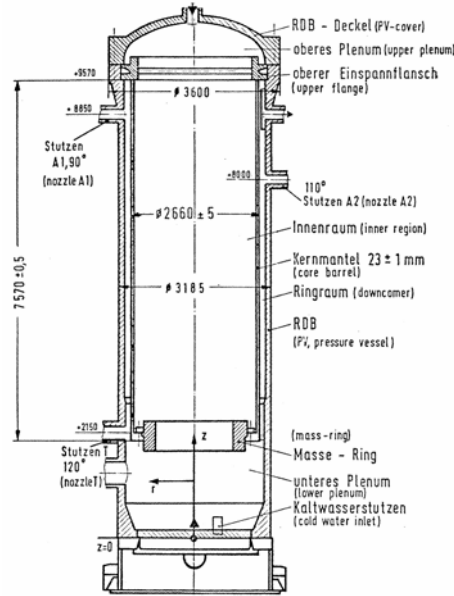


Fig. 1. HDR reactor (Wolf et al. 1983).

TABLE I  
MAIN PROPERTIES OF THE HDR BLOWDOWN EXPERIMENTS AND LOVIISA NPP

Quantity	HDR	PWR
Pressure, MPa	11	12
$p_0 - p_{sab}$ , MPa	5.5	7
$T_{core} - T_{downcomer}$ , °C	0 to 50	30
Break diameter, m	0.2	0.5
Break opening time, ms	1 to 2	
Core barrel length, m	7.6	8.1
Core barrel thickness, mm	23	50
Core barrel diameter, m	2.66	3.2
Maximum stress, MPa	100	230
Maximum displacement, mm	2	5

Blowdown experiment V32, which was the base case in the experiment series, was chosen for this work. In this experiment, the downcomer and break nozzle temperature was 240 °C and the core temperature varied axially from 308 °C at the upper core to 283 °C at the lower core barrel end. Subcooling in the downcomer and break nozzle area was quite large in the experiment V32, i.e. 78 °C which increased the loads on the core barrel.

### III. NUMERICAL MODELS

#### A. Two-phase system code simulations

The system code APROS was utilized to evaluation of the pressure boundary condition for the CFD simulation. The APROS code calculated evaporation due to flashing and fluid acceleration inside the nozzle. Because small nodes were used in the calculation, critical flow model was not applied, and the flow was calculated directly with the conservation equations of mass, momentum and energy. The external pressure boundary for APROS calculation was

adjusted with the measured pressure from the HDR experiment to get correct pressure reduction rate in the outlet of the nozzle, i.e. break opening time of 1 ms. Actual shredding out of the break disk was not simulated. Instead, a constant opening rate was assumed.

The break nozzle was modeled with 5, 15 and 45 nodes. The model with 45 nodes is depicted in Fig 2. To be able to provide a detailed time dependent pressure evolution during the first milliseconds after the break opening, the result from the case with 45 nodes was chosen as the CFD boundary condition. In this case, the node length in the break nozzle was 3 cm.

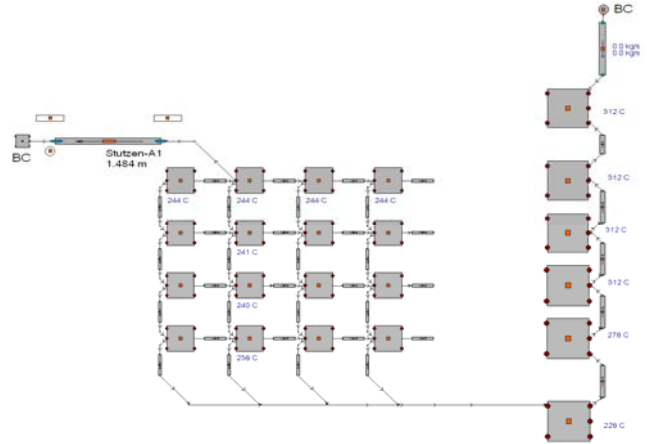


Fig. 2. APROS model.

The pressure boundary condition for the CFD calculation was taken from a point inside the nozzle where there were not yet a significant void to allow single-phase CFD simulation. Pressure in this point using 5, 15 and 45 nodes in the nozzle is plotted in Fig 3. In addition, pressure in the end of the nozzle is included from the case with 45 nodes and from the measurements. Pressure is depicted only for the first 0.01 s to show the details of the pressure drop. After  $t=0.01$  s, pressure at the break location remains almost constant. The main difference between the APROS result and the measurement is the sharp drop of pressure when the break starts to open.

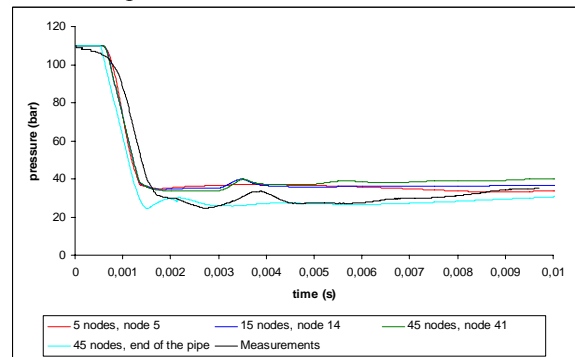


Fig. 3. Comparison to experiments. Pressure boundary condition for the CFD model.

In Fig 4, the calculated break mass flows obtained with 5, 15 and 45 nodes in the break nozzle are compared to

experimental result. In addition, the mass flow from a fully coupled FSI-simulation is included. The FSI-result is somewhat below the experiments. The difference is mainly caused by the smaller density used in the FSI-simulation.

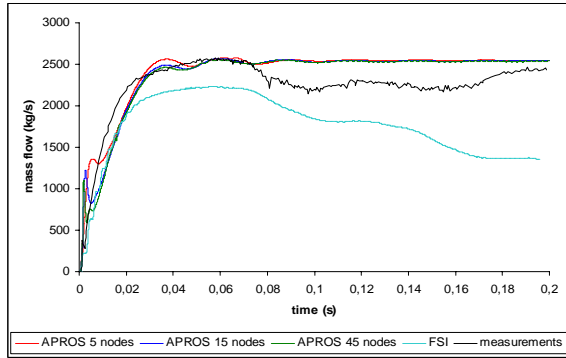


Fig. 4. Comparison to experiments. Measured and calculated blowdown flow.

### B. CFD model

Most of the simulations were performed with a CFD grid of approx 78000 grid cells. The grid is depicted if Fig 5 together with the model used in the structural solver.

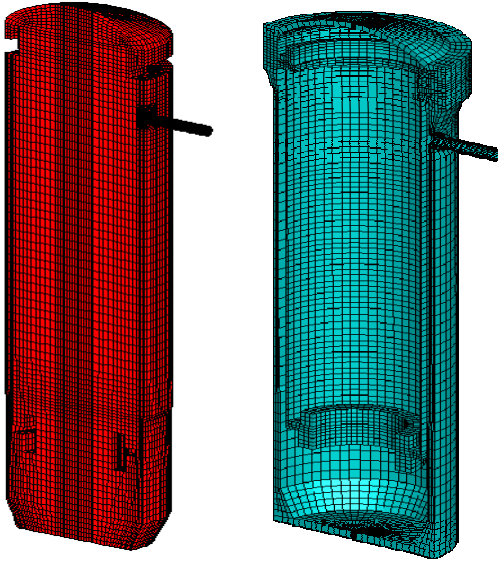


Fig. 5. Computational meshes used in the CFD (left) and structural (right) models of the HDR reactor.

In the streamwise direction, the grid resolution varies in the nozzle between 0.01 and 0.08 m and in the downcomer between 0.008 and 0.17 m. The smallest cells are located in the nozzle joint area and the largest ones in the bottom of the RPV.

On the nozzle walls,  $y^+$  values vary between  $1.5 \times 10^5$  and  $3.21 \times 10^4$  and on downcomer walls, between  $4 \times 10^4$  and 400. The largest  $y^+$  values are obtained near the nozzle joint area. On the core wall,  $y^+$  varies between 1800 and 150. Thus, the wall friction is not properly described at least in the nozzle joint area. The effect of grid resolution in this case was studied in [14], and the current grid was found adequate for description of the pressure field.

As can be seen from the experimental data, density and temperature remain almost constant during the first 0.20 s after the pipe break. Thus in the present simulations, a constant temperature corresponding to the average of maximum and minimum temperatures obtained in the measurements ( $274^\circ\text{C}$ ) was assumed in most of the simulations. The corresponding dynamic viscosity is  $\mu=0.0001\text{Pa}\cdot\text{s}$ .

Fluent and Star-CD are both finite-volume based CFD solvers. In both codes, the pressure-based solver was utilized which is a standard choice in flows with low Mach number. The PISO pressure-correction method was applied. In the present application, water has to be treated as a compressible fluid. Thus, in the mass-balance equation, the non-constant density has to be accounted for, and this modifies the pressure-correction equation. In the pressure correction step, the correction of the mass flow,  $\Delta m$ , is written as

$$\Delta m = \Delta(A\rho u) = \rho\Delta(Au) + (Au)\Delta\rho \quad (1)$$

where  $A$  is the cross-sectional flow area,  $\rho$  the density and  $u$  the flow velocity. The change of density,  $\Delta\rho$ , is evaluated using the change of pressure,  $\Delta p$ , and the compressibility of water,  $\kappa$ , as

$$\Delta\rho = \kappa\rho\Delta p \quad (2)$$

The value for density is calculated using pressure as

$$\rho = \rho_0 + \kappa\rho_0(p - p_0) \quad (3)$$

The applied reference values were  $\rho_0 = 758.5 \text{ kg/m}^3$ ,  $p_0 = 110 \text{ bar}$  and  $\kappa = 1153.9 \times 10^{-12} \text{ Pa}^{-1}$ . For more details on the pressure correction methods for compressible fluids see e.g. [15].

In the CFD model, the so-called standard  $k-\epsilon$  turbulence model of Launder and Sharma with the standard wall functions was applied [11]. The solid walls were treated as viscous walls using wall functions. At the break nozzle, the pressure outflow condition was applied, and the static pressure obtained from the APROS simulation or from the experiment was set on this boundary.

The simulations were also run using the pressure boundary condition from the experiment. Although the pressure drop is sharp in the APROS result (see Fig 3), changing the boundary condition had only a small effect on the obtained pressure field and displacement.

In simulations with Fluent, the first-order implicit time-integration method is the only available option when the mesh is deforming. The time step was set to  $10 \mu\text{s}$ , which, in this case, corresponds to Courant number ( $\Delta t c/\Delta x$ ,  $c$ =speed of sound) of 0.1 or below.

The convective terms in the equations of momentum and turbulence quantities were discretized using the third-order MUSCL scheme of Fluent and the diffusion terms with a second-order central-difference scheme (see [11]). Both second and first-order discretization was applied to pressure, but this did not affect the obtained pressure field.

In simulations using Star-CD, the Crank-Nicolson method

was applied to the temporal discretization. For the spatial discretization, the Monotone Advection and Reconstruction Scheme (MARS) was used for velocities, central differencing for turbulence quantities and blended central-upwind differencing with blending factor 0.7 for density. [9]

### C. Structural model

In the finite-element based structural solver Abaqus, a linear finite-element model of the reactor with about 15000 8-node hexahedral elements was applied. Continuum shell elements, which have only displacement degrees of freedom but model shell behavior accurately, were mainly used. Conventional solid elements were used in a few necessary regions. One layer of continuum shell elements was used in the core barrel wall and four layers in the RPV wall. The mesh of the structural model is shown in Fig 5. The structural model had a preliminary static load step in which the static pressure condition was achieved. After the static load step, applied pressure was provided by CFD code.

Material properties  $E = 175$  GPa,  $\nu = 0.3$  and  $\rho = 7900$  kg/m<sup>3</sup> were used for elastic modulus, Poisson's ratio and density of the core barrel, respectively. For the RPV, values  $E = 190$  GPa,  $\nu = 0.3$  and  $\rho = 7850$  kg/m<sup>3</sup> were applied. A small amount of stiffness proportional Rayleigh damping was included in the RPV wall. Value  $\beta = 6 \times 10^{-6}$  was used which results in 2 % of critical damping at frequency 1000 Hz. The maximum frequency of interest was estimated as 400 Hz.

### D. Coupling of CFD and structural models

The external coupling software MpCCI was applied to bidirectional coupling of the CFD and structural solvers. In this approach, the CFD and structural analysis codes run simultaneously and coupling information is exchanged during the simulation. Interpolation is used for transferring coupling quantities between the fluid and structure meshes. In this work, the coupling quantities were fluid pressure and nodal coordinates of the structure, and the codes exchanged information in the beginning of each time step. The simulations were run on a PC with Intel Core 2 CPU 1.86 Ghz processor in the Windows environment. A simulation for the time period  $t=0$  to 0.20 s took approximately 96 hours of wall clock time. The fully coupled simulation took approximately 33% more CPU time than a simulation with one-way pressure mapping. The increased computation is mainly caused by moving the RPV walls in Fluent, and communication between the codes does not seem to significantly increase the CPU time.

## IV. SIMULATION RESULTS

### A. Bidirectional FSI simulations

In the cases discussed in this subsection, the computational grids depicted in Fig 5 was applied. The pressure boundary condition was taken from the APROS result and temperature had the constant value of 274°C. The modeling details in Fluent and Star-CD were chosen as close

to each other as possible, but as discussed in section III.B, there were some differences in the numerical methods. Propagation of the pressure wave and the resulting stress and displacement are demonstrated in Fig 6 and Fig 7. In the figures depicting the stress, the deformation is scaled by the factor of 200.

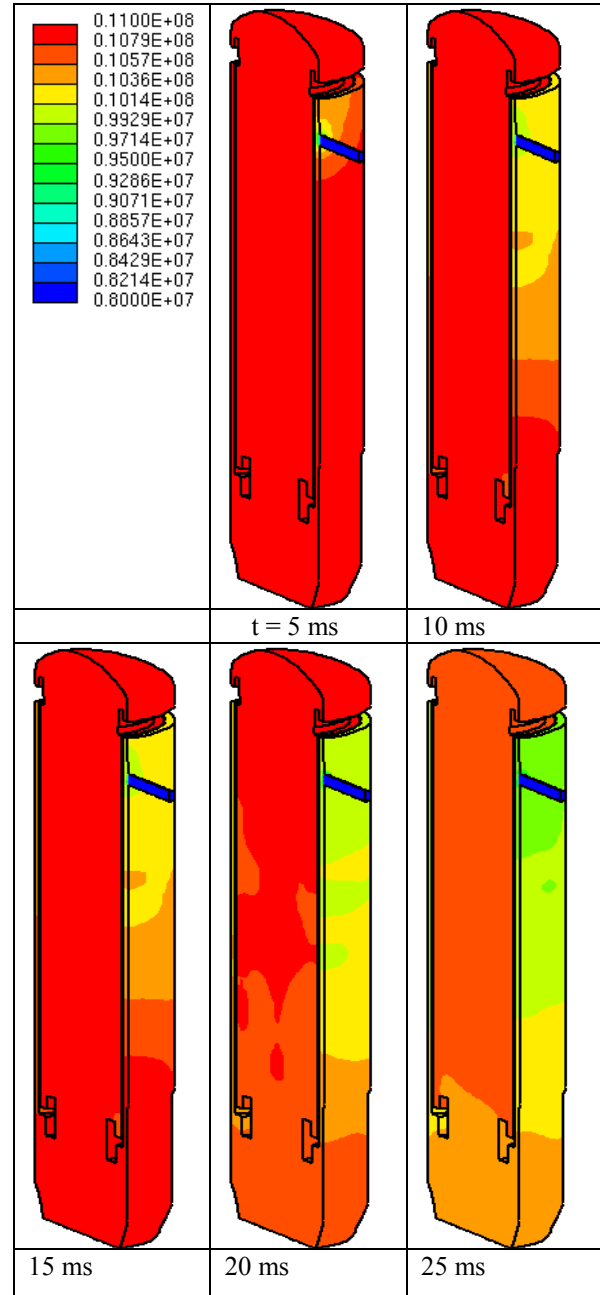


Fig. 6. Pressure in the CFD model

Pressure on the inner wall of the downcomer at the nozzle location (in cylindrical coordinates of Fig 1 at  $\varphi=90^\circ$ ,  $z=8.85$ m) and somewhat below the nozzle ( $\varphi=90^\circ$ ,  $z=2.3$ m) are depicted in Fig 8 and Fig 9, respectively. Pressure on the opposite side of the downcomer ( $\varphi=270^\circ$ ,  $z=7.78$ m) is given in Fig 10 and pressure on the core axis in Fig 11. The pressure field is slightly underpredicted by both simulations,

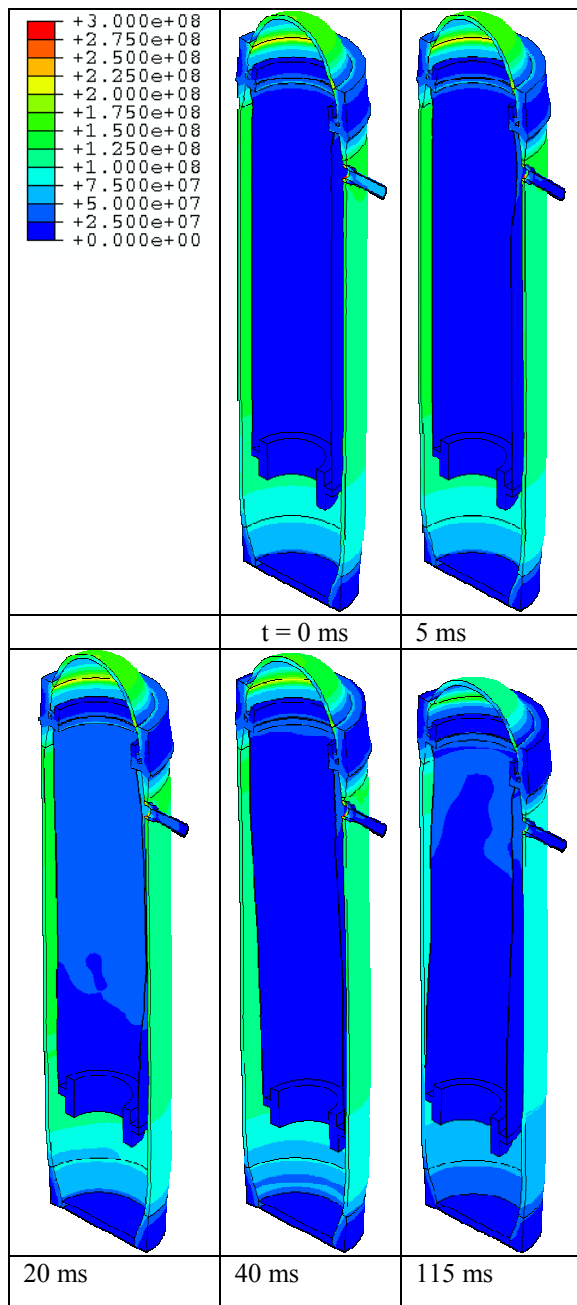


Fig. 7. Von Mises stress, displacements are scaled with the factor of 200

but it follows the experiments fairly well until approximately  $t=0.1$  s. After this, flashing occurs [5] and the one-phase model fails to describe the flow. During the first 20 ms, both simulations predict an oscillation of approximately 380 Hz in the pressure field. This frequency corresponds to a pressure wave travelling back and forth in the nozzle. The oscillation is not shown in the experiment which may be caused by boiling inside the nozzle (and outside it) which makes the water “soft” in this region.

The pressure on both sides of the wall of the core barrel is underpredicted in a similar manner. Because of this, the pressure difference across the wall follows the experiment even better than the wall pressure. This is visible in the resulting relative displacements between the walls of the

core barrel and RPV which are depicted on several locations of the downcomer wall in Fig 12-Fig 15. Here, we notice that the displacements are predicted fairly well for the entire duration of the simulations.

The Hoop strain and the axial strain on the wall of the core barrel are shown in Fig 16 - Fig 19. The strain oscillates with the frequency corresponding to the pressure wave travelling in the nozzle. This frequency was also visible in the pressure field. The result obtained with Star-CD oscillates clearly more than the one obtained with Fluent which is caused by different time-integration methods.

The two CFD solvers produce almost identical results. However, the Fluent result is somewhat smoother. Since the same computational grid and pressure boundary condition were applied in the simulations with Fluent and Star-CD, the main difference between the two models is in the numerical methods. Based on the results of this subsection, we can conclude that the results are not strongly sensitive to numerical methods.

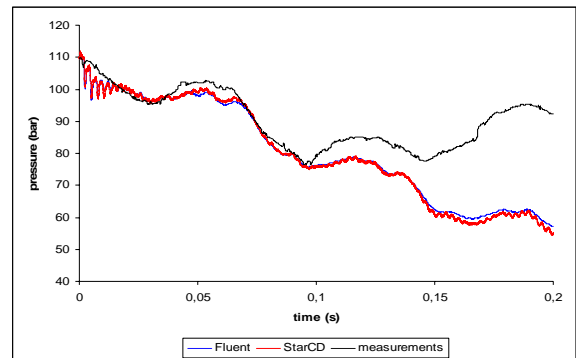


Fig. 8. Pressure on the inner downcomer wall at  $\phi=90^\circ$ ,  $z=8.85$ m.

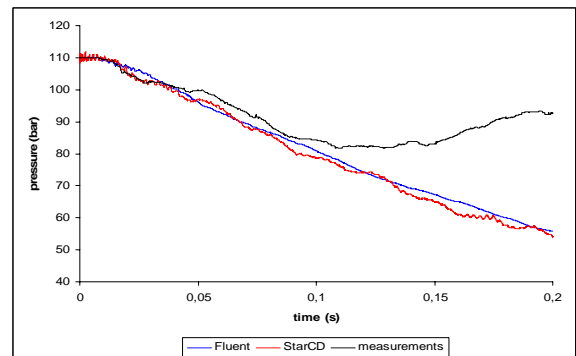


Fig. 9. Pressure on the inner downcomer wall at  $\phi=90^\circ$ ,  $z=2.3$ m.

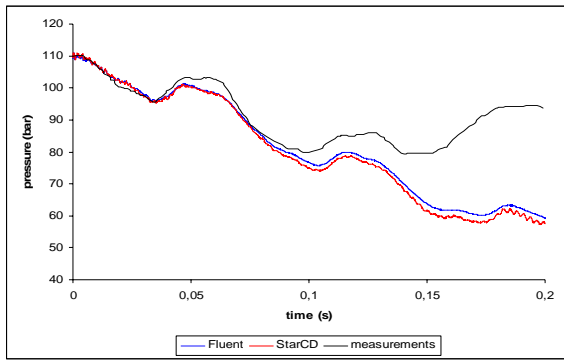


Fig. 10. Pressure on the inner downcomer wall at  $\varphi=270^\circ$ ,  $z=7.78\text{m}$ .

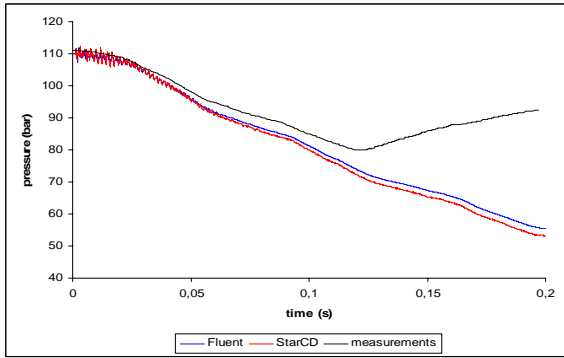


Fig. 11. Pressure on the core axis at  $\varphi=270^\circ$ ,  $z=5.05\text{m}$ .

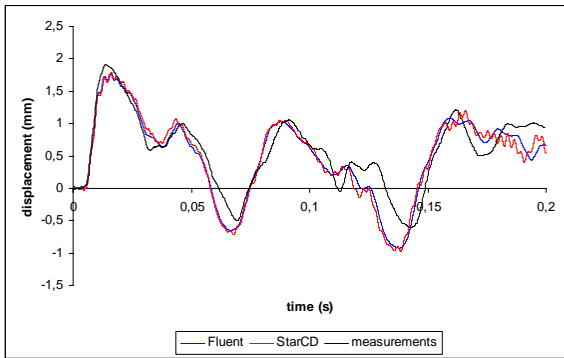


Fig. 12. Relative radial displacement between the core barrel and RPV at  $z=7.15\text{m}$ ,  $\varphi=90^\circ$ .

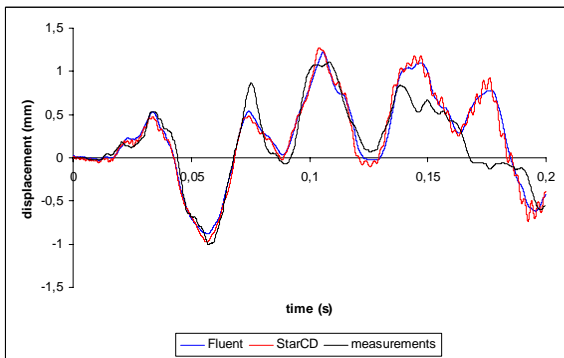


Fig. 13. Relative radial displacement between the core barrel and RPV at  $z=7.15\text{m}$ ,  $\varphi=270^\circ$ .

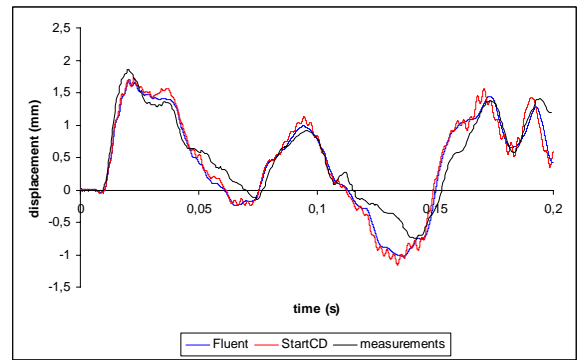


Fig. 14. Relative radial displacement between the core barrel and RPV at  $z=5.55\text{m}$ ,  $\varphi=90^\circ$ .

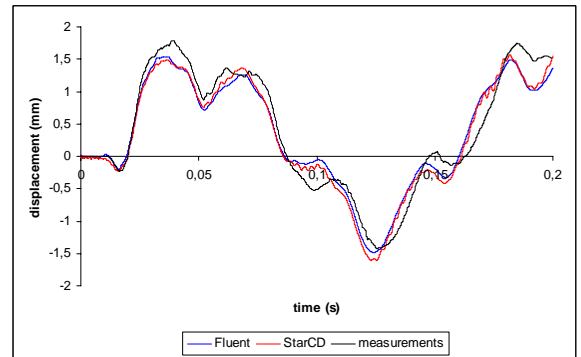


Fig. 15. Relative radial displacement between the core barrel and RPV at  $z=2.3\text{m}$ ,  $\varphi=90^\circ$ .

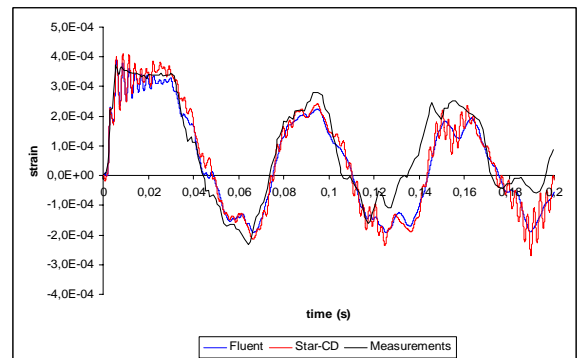


Fig. 16. Hoop strain on the outer surface of the core barrel at  $z=8.85$ ,  $\varphi=90^\circ$ .

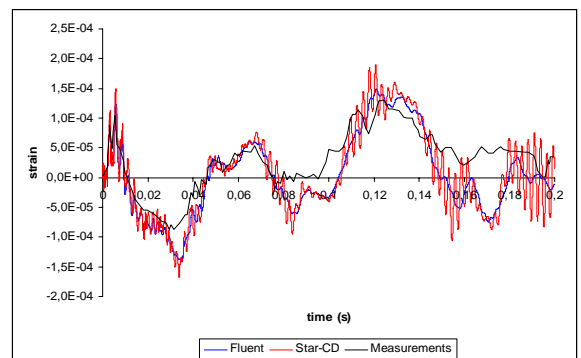


Fig. 17. Axial strain on the outer surface of the core barrel at  $z=8.85$ ,  $\varphi=90^\circ$ .



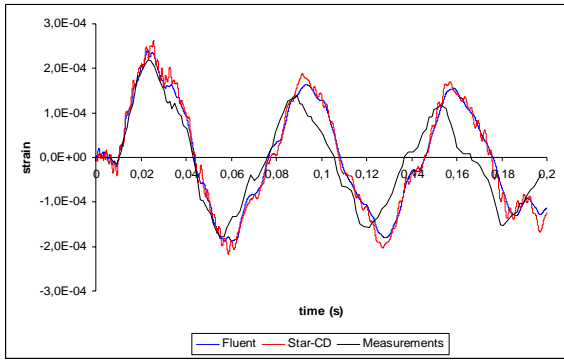


Fig. 18. Hoop strain on the inner surface of the core barrel wall  $z=8.85$ ,  $\varphi=135^\circ$ .

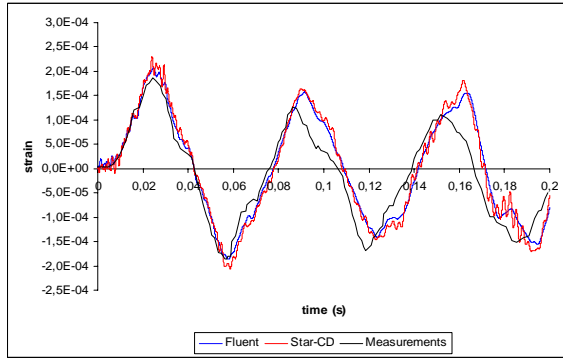


Fig. 19. Hoop strain on the inner surface of the core barrel wall  $z=8.85$ ,  $\varphi=225^\circ$ .

### B. Effect of water temperature

To study the sensitivity of the obtained pressure field to the water temperature, the simulation was repeated at the maximum and minimum temperatures of the experiment, i.e.  $308^\circ\text{C}$  and  $240^\circ\text{C}$ . In the pressure-based solver applied in the present work, pressure is solved from the mass conservation equation (Section III.B), and the effect of temperature is seen in water density and speed of sound.

The obtained pressure field on the wall of the downcomer together with the experimental result and the result from the previous section are depicted in Fig 20. We notice that the pressure field varies somewhat with temperature. However, the present implementation of the compressible pressure correction method does not allow temperature dependent speed of sound or density, and it was not possible to give a temperature distribution. Thus, assuming the average temperature was the best available estimate.

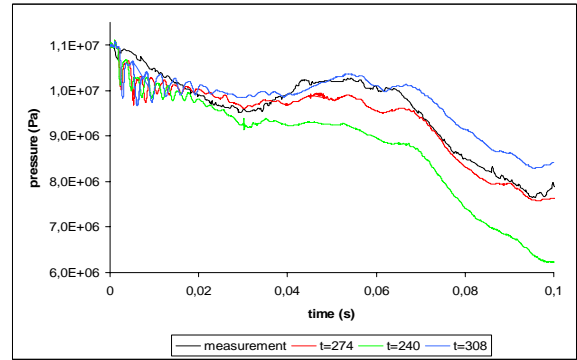


Fig. 20. Effect of water temperature. Pressure on the downcomer wall at  $z=8.85\text{m}$ ,  $\varphi=90^\circ$ .

### C. Time-integration method with one-way mapping and bidirectional coupling

In Fluent, the first-order time-integration method is the only available option when the mesh is deforming. Because of this, the effect of the order of the time-integration method was studied using one-way pressure mapping where the walls of the CFD model remain rigid. These results also demonstrate the necessity of using bidirectional coupling.

The pressure obtained using one-way pressure mapping, bidirectional coupling and measurements is depicted in Fig 21 and displacement in Fig 22. In case with bidirectional coupling, wall movement damps the pressure oscillation. With one-way pressure mapping, the pressure field does not react to the wall movement of the structural model, and the obtained displacements differ considerably from the measurement. The differences between the one-way pressure mapping and bidirectional coupling are similar to those obtained in [5] where a simpler model was used for the flow field.

The order of the time-integration method affects the damping of the pressure fluctuation, but it has only a small effect on the general behavior of the pressure field. The case with bidirectional coupling was repeated using the time step of  $2.5 \mu\text{s}$ . The effect of time step size is most clearly visible in the strain which is depicted in Fig 23.

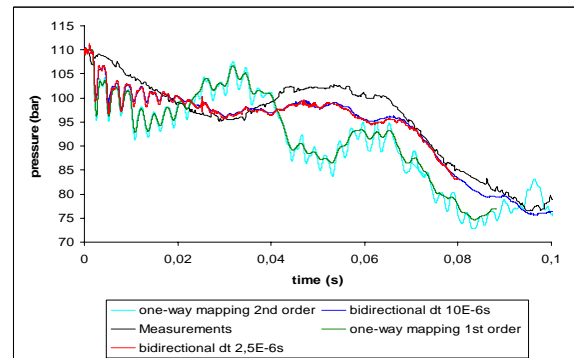


Fig. 21. Effect of time integration method with one-way pressure mapping and bidirectional coupling. Pressure on the downcomer wall at  $z=8.85\text{m}$ ,  $\varphi=90^\circ$ .

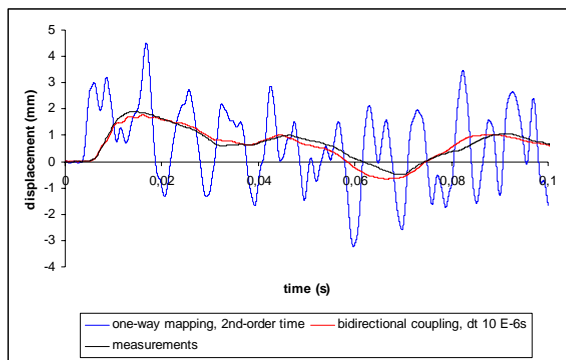


Fig. 22. Effect of FSI. Relative radial displacement between the core barrel and RPV at  $z=7.15\text{m}$ ,  $\varphi=90^\circ$ .

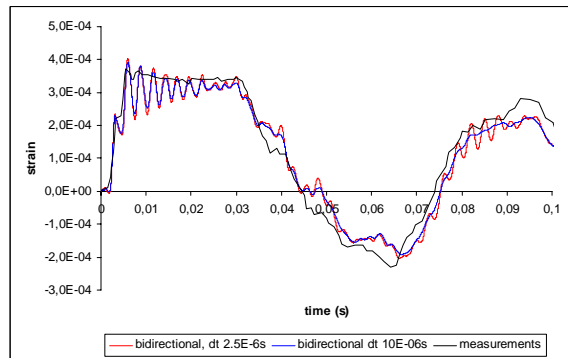


Fig. 23. Effect of time step size. Hoop strain on the outer surface of the core barrel at  $z=8.85$ ,  $\varphi=90^\circ$ .

## V. CONCLUSION

In this article, we have presented results from simulations of the pressure transient occurring in the early phase LBLOCA. The results were obtained by bidirectional coupling of CFD and structural solvers. The pressure boundary condition was obtained in a two-phase system code simulation with APROS. The main aim of this work was to validate the simulation environment against the HDR experiments and to describe the sensitivity of the results to pressure boundary condition, numerical methods and grid resolution.

The assumption of one-phase flow used in the CFD model was valid until approximately  $t=100$  ms and after this, the pressure field clearly deviated from the experimental result. During the first 100 ms, the obtained pressure field was fairly close to the experiments. The pressure on both sides of the core barrel was underpredicted in a similar manner, and thus the pressure difference, which determines the wall movement, followed the experimental result even better. In addition, the pressure difference was not as sensitive to flashing as the wall pressure and the wall displacement was predicted quite accurately for the entire simulation, i.e. until  $t=200$  ms.

The obtained pressure field was not sensitive to pressure boundary condition or numerical methods of the CFD model. Some sensitivity of the pressure field to temperature was obtained, and accounting for non-constant temperature will be studied in the future work.

Based on the present results, we can conclude that the simulation environment is capable of simulating the FSI phenomena related to the early phase of LBLOCA where the flow can be considered as a one-phase flow.

## REFERENCES

- [1] *MpCCI 3.0.6-12 Documentation User manual*, Fraunhofer Institute for Algorithms and Scientific Computing SCAI, Germany, 2007.
- [2] APROS, *The Advanced Process Simulation Environment*, <http://apros.vtt.fi/>, Technical research centre of Finland.
- [3] L. Wolf, *Design report for the HDR-RPV-I blowdown experiments V31.2, V32, V33 and V34 with specifications for the pretest computation*, HDR Safety Program, Report No. 3.243/81, Kernforschungszentrum Karlsruhe, 1981.
- [4] L. Wolf, "Experimental results of coupled fluid-structure interactions during blowdown of the HDR-vessel and comparisons with pre- and post-test predictions", *Nuclear Engineering and Design*, 70, 269–308, 1982.
- [5] L. Wolf, M. Schall, and H. Bader, *Untersuchungen von RDB-Einbauten bei Bruch einer Reaktorkühlmittelleitung*, HDR Sicherheitsprogramm, Technischer Fachbericht 29-82, Kernforschungszentrum Karlsruhe, 1983.
- [6] L. Andersson, P. Andersson, J. Lundwall, J. Sundqvist, K. Nilsson and P. Veber, "On the validation and application of fluid-structure interaction analysis of reactor vessel internals at loss of coolant accident", *Computers & Structures*, 81, 469-476, 2003.
- [7] V. Lestinen, T. Toppila, A. Timperi, T. Pättikangas and M. Hänninen, "Determination of thermal-hydraulic loads on reactor internals in a DBA-situation", in *ASME Pressure Vessels and Piping Conference*, Vancouver, Canada, July 23-27 2006, PVP2006-ICPVT11-93456, 2006.
- [8] F. Casadei and S. Potapov, "Permanent fluid-structure interaction with non-conforming interfaces in fast transient dynamics", *Computer methods in applied mechanics and engineering*, 193, 4157-4194, 2004.
- [9] A. Timperi, T. Pättikangas, I. Karppinen, V. Lestinen, J. Kähkönen and T. Toppila, "Validation of fluid-structure interaction calculations in a large-break loss of coolant accident", in *Proc. of the 16th International Conference on Nuclear Engineering ICONE16*, Orlando, Florida, USA, May 11-15 2008, 2008.
- [10] CD adapco Group, *Star-CD Version 3.20, Methodology*, 2004.
- [11] *Fluent 6.3 Documentation, User's guide*, Fluent inc, 2007.
- [12] *Abaqus/CAE 6.7 User's manual*, Dassault systems simulia corp. 2007.
- [13] M. Schall, *Untersuchungen von RDB-Einbauten bei Bruch einer Reaktorkühlmittelleitung*, HDR Sicherheitsprogramm, Technischer Fachbericht 48-84, Kernforschungszentrum Karlsruhe, 1984.
- [14] T. Brandt, V. Lestinen, J. Kähkönen, T. Toppila, A. Timperi, T. Pättikangas, and I. Karppinen, "Fluid-Structure interaction analysis of large-break loss of coolant accident" in *Proc of Experiments and CFD code application to Nuclear Reactor Safety, XCFD4NRS*, Grenoble, France, September 10-12, 2008.
- [15] J. H. Ferziger, M. Perić: "Computational Methods for Fluid Dynamics", 2nd edition, Springer, 1999.